DOI: 10.1002/smll.200700187

Morphology Control of Structured Polymer Brushes

Marin Steenackers, Alexander Küller, Nirmalya Ballav, Michael Zharnikov, Michael Grunze, and Rainer Jordan**

The surface-initiated photopolymerization (SIPP) of vinyl monomers on structured self-assembled monolayers, as defined by two-dimensional (2D) initiator templates for polymer growth, is investigated. The 2D templates are prepared by electron-beam chemical lithography (EBCL) of 4′-nitro-4-mercaptobiphenyl (NBT) and chemical conversion to an asymmetric azo initiator (4′-azomethylmalonodinitrile-1,1′-biphenyl-4-thiol). Ex situ kinetic studies of the SIPP process reveal a linear increase in the thickness of the polymer layer with the irradiation/polymerization time. The effect of the applied electron dosage during the EBCL process upon the final thickness of the polymer layer is also studied. The correlation between the electron-induced conversion of the 4′-nitro to the 4′-amino group and the layer thickness of the resulting polymer brush indicates that the polymer-brush grafting density can be directly controlled by the EBCL process. NBT-based template arrays are used for the combinatorial study of the influence of the lateral structure size and the irradiation dosage on the morphology of the resulting polymer-brush layer. Analysis of the array topography reveals the dependence of the thickness of the dry polymer layer on both electron dosage and structure size. This unique combination of EBCL as a lithographic technique to locally manipulate the surface chemistry and SIPP to amplify the created differences allows the preparation of defined polymer-brush layers of controlled morphologies.

Keywords:
- kinetics
- lithography
- polymer brushes
- polymerization
- self-assembled monolayers

1. Introduction

Surface-initiated polymerization (SIP) has been widely used for the preparation of dense and well-defined polymer brushes on solids.[1] This concept has been demonstrated for all types of polymerization including free[2] and controlled[3] radical, living anionic,[4] and living cationic[5] polymerization. Precise control of the grafting location, brush density, and thickness of the polymer brushes can be realized by using a monomolecular template provided by self-assembled monolayers (SAMs) bearing the initiator sites as surface-bonded two-dimensional (2D) initiator systems. SAM systems also offer the possibility to control the lateral distribution of the

[*] Dr. A. Küller, Dr. N. Ballav, Dr. M. Zharnikov, Prof. M. Grunze
Lehrstuhl für Angewandte Physikalische Chemie
Universität Heidelberg
Im Neuenheimer Feld 253, 69120 Heidelberg (Germany)
Fax: (+49) 6221-54-6199
E-mail: Michael.Grunze@urz.uni-heidelberg.de
M. Steenackers, Dr. R. Jordan
Wacker-Lehrstuhl für Makromolekulare Chemie
Technische Universität München
Lichtenbergstr. 4, 85747 Garching (Germany)
Fax: (+49) 89-289-13562
E-mail: Rainer.Jordan@ch.tum.de

Supporting information for this article is available on the WWW under http://www.small-journal.com or from the author.

small NANO MICRO

grafting sites by various techniques, such as microcontact printing,[6] 2D gradients,[7] or scanning probe microscopy based techniques.[8]

Recently, we reported the synthesis of patterned polymer brushes on the micro- and nanometer scales by combining so-called electron-beam chemical lithography (EBCL)[9,10] on SAMs of 4′-nitro-4-mercaptobiphenyl (NBT) on gold, and amplification of the primary structure by radical SIP of styrene.[11] The reaction scheme, which starts from a homogeneous SAM of NBT and ends with SIP on structured 2D azo initiator systems, is outlined in Figure 1. The irradiation-induced crosslinking of the biphenyls enhances the stability of the monolayer due to the multiple adhesion sites of the entire layer, which allows polymerization at elevated temperatures as well as by UV irradiation.[12] Recently, the preparation of freestanding nanosheets of SAMs of the crosslinked biphenyl was demonstrated.[13]

While larger SAM areas can be structured by EBCL using an electron flood gun in combination with a stencil mask, much smaller and more complex structuring can be fabricated by "direct writing" with a focused electron beam (e-beam). In combination with SIPP, micro- and nanometer-sized structures can be prepared side by side on a single substrate.[14] This opens the possibility to study the effect of various chemical or physical parameters on the brush properties by creating arrays of structures or polymer-brush gradients on a single substrate. The advantage of this combinatorial approach was first impressively demonstrated by Genzer and co-workers,[15] who fabricated gradient polymer-brush systems with a continuous variation of polymer chain length, grafting density, (block) copolymer composition, and so on. Since then, many research groups have taken advantage of the combinatorial approach by fabricating and using gradients or arrays of structured polymer brushes[16–19] to study various properties of the brush surface, as well as the impact of synthetic or compositional parameters on the morphology and properties of the brush gradients, or to perform high-throughput screening for tissue compatibility.[19] With the reported experimental techniques, such as continuous removal/immersion of the reactive substrate into a monomer solution or use of a moving shutter during photopolymerization, the lateral dimensions of gradients are at the macroscopic scale. Much smaller array features, in which the structural dimensions approach the dimensions of the grafted macromolecules, can be prepared by the combination of EBCL and SIP, as demonstrated by Zauscher and co-workers[20,21] and by us.[11,14]

Besides variation of the chemical composition of the polymer brush, the morphology and topography of the brush layer determines the overall properties of the polymer coating. Here, we studied the dependence of the thickness of the dry polymer layer on the polymerization time (at $\lambda_{max} = 350$ nm) in a complete set of experiments on individual samples. Moreover, we studied the influence of the applied electron dosage and the characteristic structure size (50–1000 nm) on the height and morphology of the resulting polymer brushes in a combinatorial approach.

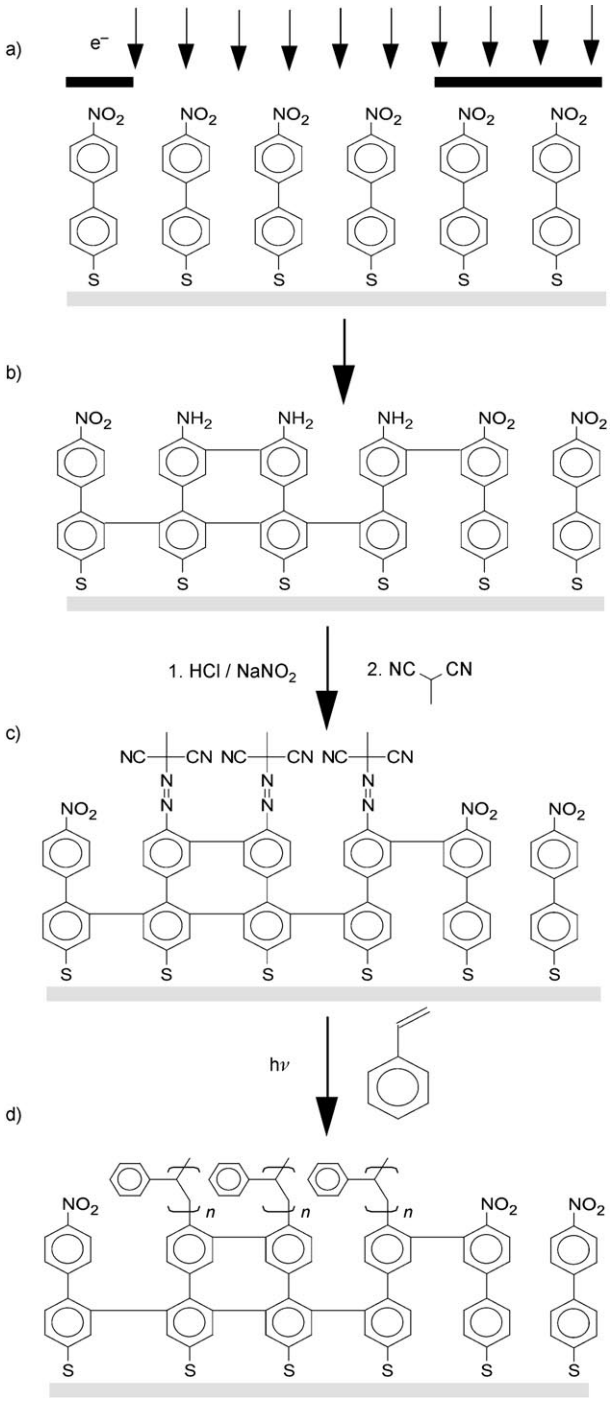

Figure 1. a) Electron-beam irradiation of NBT SAMs on Au(111) through a stencil mask or by direct writing with a focused electron beam. b) Crosslinking of the biphenyl moieties with simultaneous conversion of the nitro to the amino-group results in structured SAMs of 4′-amino-1,1′-biphenyl-4-thiol (cABT). c) Diazotization and coupling with malonodinitrile gives a 4′-azomethylmalonodinitrile-1,1′-biphenyl-4-thiol (cAMBT) SAM that bears an asymmetric azo initiator. d) SIP by exposure to a vinyl monomer and heating or UV irradiation results in a patterned polymer-brush layer.

2. Results and Discussion

The asymmetric surface-bound azo compound 4′-azomethylmalonodinitrile-1,1′-biphenyl-4-thiol (cAMBT), formed after EBCL and wet chemical conversion (Figure 1), is suitable for the thermal[22] and photochemical[22,23] SIP of a broad variety of vinyl monomers. Recently, we investigated the effect of the polymerization conditions (temperature and irradiation wavelength) on the increase in the thickness of the polymer layer as a function of the reaction time.[24] It was shown that the SIPP of styrene at room temperature leads to denser, more homogeneous, and significantly thicker polymer brushes as compared to the thermally initiated SIP. Furthermore, it was found that using an irradiation source for the SIPP with wavelength below $\lambda = 300$ nm caused the degradation of polystyrene brushes and maximum layer thicknesses were found to be around 10–20 nm.

Our preliminary results demonstrated that SIPP by irradiation with light of a spectral distribution between 300 and 400 nm ($\lambda_{max} = 350$ nm) leads to much thicker polymer brushes. Figure 2 shows an atomic force microscopy (AFM) image of a typical polymer structure obtained by EBCL using a stencil mask with circular openings of radius 1 μm and polymerization of styrene with a UV irradiation time of $t_P = 10$ h. The SIPP resulted in well-defined polymer-brush patterns. As for the thermally initiated SIP or the SIPP at $\lambda_{max} = 300$ nm, polymer structures selectively grew on the electron-irradiated areas; however, since no polymer photolysis occurred, the layer thicknesses are significantly greater.

Ex situ kinetic studies of individual samples at different UV irradiation times (2–24 h) revealed an almost linear relationship between the thickness of the dry polymer brush and the duration of the irradiation, up to a thickness of ≈200 nm achieved after irradiation for 20 h (Figure 3).

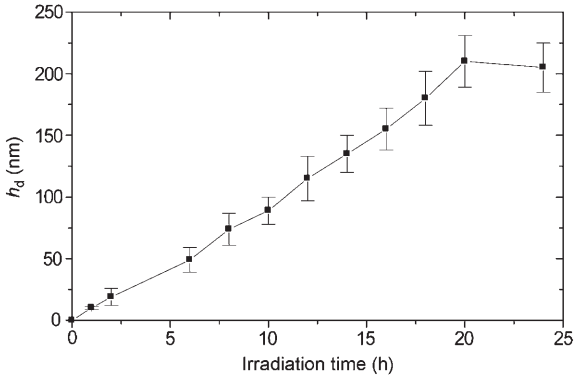

Figure 3. Thickness of the dry polymer layer h_d as a function of UV irradiation time ($\lambda_{max} = 350$ nm) as measured by AFM on structured polymer brushes (1-μm radius, 4-μm spacing, EBCL at 50 eV; electron dosage: 60 mC cm^{-2}).

Longer irradiation times did not result in a further increase of the layer thickness. Under these conditions, we observed that the bulk monomer phase became highly viscous. This indicates significant polymer content in the monomer phase due to the autoinitiated polymerization of styrene in solution under UV irradiation. The limited film growth can therefore be explained by either the limited mass transport of the remaining monomer and/or the higher termination rate by combination of radical chain ends in solution and on the surface. Experiments with an irradiation time over 30 h could not be performed due to the solidification of the reaction mixture.

In contrast to the findings of Dyer et al.,[25,26] who proposed a four-stage growth model for the SIPP of styrene on azobisisobutyronitrile (AIBN)-type initiators, no significant deviation from this linear thickness increase at UV irradiation times ranging from 0 to 20 h could be observed. Our findings are similar to those of Rühe et al.[23] who also observed a linear thickness increase. Note, however, that both experimental setups (light source, reaction vessels, irradiation geometry) and initiator systems and UV intensity (Dyer et al.: 1.6 mW cm^{-2}; Rühe et al.: 30 mW cm^{-2}; here: 9.2 mW cm^{-2}) are dif-

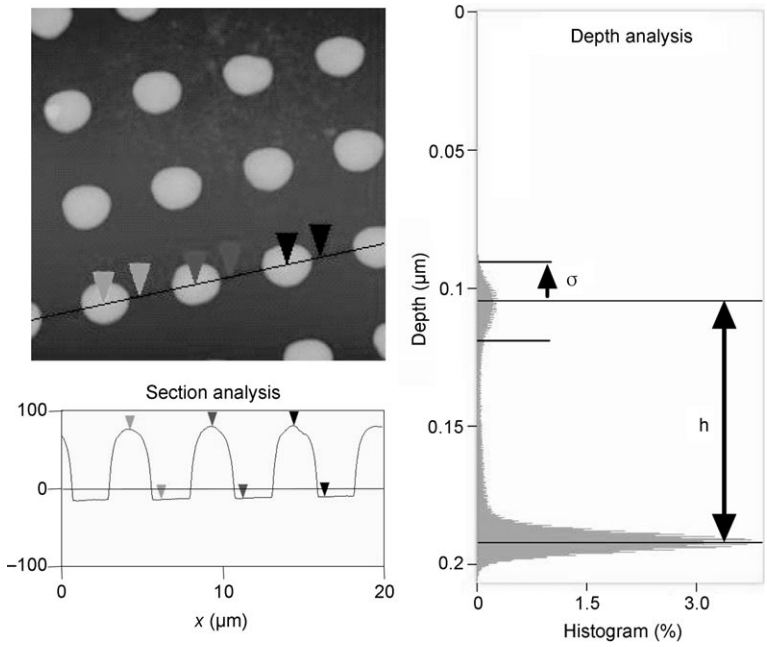

Figure 2. AFM image, height profile along the black line shown in the image, and depth analysis of patterned polystyrene brushes (20 × 20 μm^2). SIPP by UV irradiation ($\lambda_{max} = 350$ nm). Irradiation time: 10 h. Depth analysis of the scan gives an average height (h) and standard derivation (σ) of the polymer layer thickness.

ferent in the three experiments and may influence not only the growth rate but also the growth characteristics.

Besides the polymerization of styrene, this SIPP reaction can be used for any vinyl monomer that can be polymerized by free-radical polymerization. Up to now, we have successfully tested methyl methacrylate (MMA) and acrylic acid (AAc). However, the increase of the thickness of the dry polymer layer h_d with the irradiation time was found to be specific for each monomer. The differences in thickness growth rate correlate roughly with the rate of polymerization of the monomers in solution. For example, after 3.5 h of irradiation, SIPP of MMA gave layer thicknesses of 120 nm and after only 10 min AAc gave a brush thickness of 290 nm. However, a systematic study of the kinetics for these monomers was not performed.

Notably, the presented process for the fabrication of structured polymer layers proved to be very reliable in terms of the reproducibility of the locus and thickness of the polymer layers on the substrate. However, in some experiments we noticed deviations in the morphology of individual polymer structures, that is, that the thickness of the polymer layer varies to some extent within a single pattern feature. Especially at the outer edges of the patterned field, we noticed the formation of "soft-boiled egg" shapes (Figure 4b) instead of the regular dots (Figure 4a). Closer inspection revealed that these complex polymer structures were caused by local inhomogeneous electron irradiation of the NBT SAM (i.e., interference at mask edges with a considerable gap between mask and substrate); the existence of such interference has been previously demonstrated by X-ray absorption spectromicroscopy.[27] This finding indicates a direct dependence between the thickness of the polymer layer and the locally applied electron dosage.

To study the influence of the electron dose during EBCL on the thickness of the resulting polymer brush, we prepared a "gradient surface" on which the electron dose was continuously increased within a defined area, instead of irradiation of a large number of individual areas with different irradiation dosages. Apart from being faster, this approach guarantees that all further reaction parameters remain constant. This was performed with a focused e-beam of a scanning electron microscope (SEM) coupled to a pattern generator (direct e-beam writing).

Figure 5 displays an AFM image of the resulting polymer structure (width 10 μm; length 50 μm) along with the gradient of the applied electron dosage from 0 to 115 mC cm^{-2} and the corresponding height profile along the gradient direction. Figure 6 shows a detailed view of the same structure at the onset of the gradient prepared with electron dosages from 0 to 20 mC cm^{-2}. Clearly, the height of the resulting polymer brush can be directly controlled by the applied electron dosage for the reductive conversion of NBT to the cABT monolayer within the EBCL step. As outlined in Figure 1, the consecutive conversion by diazotization of cABT and coupling of cAMBT is only possible for the reduced cABT form and only there can SIPP occur. In the polymer-brush regime, the thickness of the dry brush layer h_d scales not only with the degree of polymerization but also with the grafting density (polymer-brush conditions:

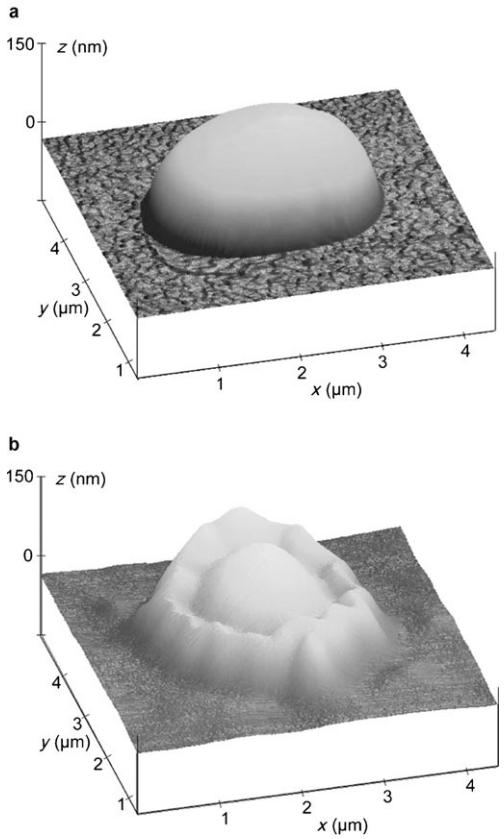

Figure 4. Three-dimensional representations of AFM images of the polystyrene dots. The structures were generated by electron irradiation of an NBT SAM using a stencil mask with a circular opening of radius 1 μm and subsequent SIPP in the presence of bulk styrene at $\lambda_{max} = 350$ nm. a) Structure obtained after homogeneous electron irradiation of an NBT SAM. b) Polystyrene dot with a "soft-boiled egg" shape caused by inhomogeneous electron irradiation.

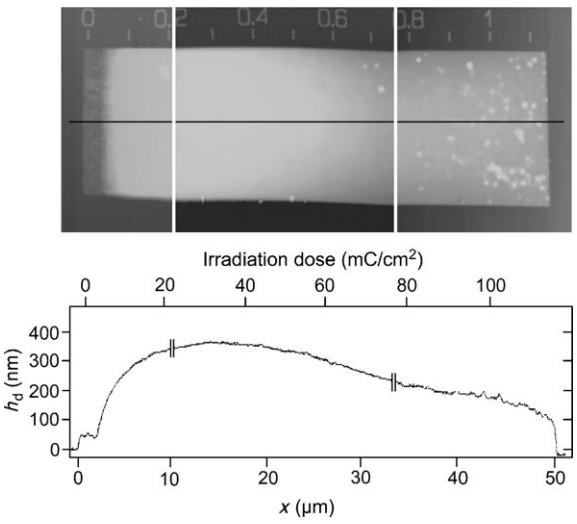

Figure 5. AFM image and height profile of a polystyrene grafting-density gradient. The image was recorded by three individual scans for better resolution. The measurement was performed in tapping mode under ambient conditions. The electron dosage for the EBCL was linearly increased from 0 to 115 mC cm^{-2} going from left to right, as indicated by the scale bar at the top of the AFM image.

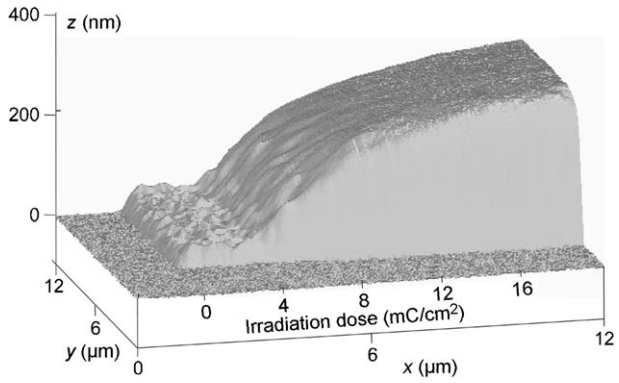

Figure 6. Three-dimensional plot of the AFM height image of the gradient polymer brush shown in Figure 5 for a dose range of 0–20 mC cm^{-2}.

$h_d = M_n \sigma / \rho N_A$, where M_n, σ, ρ, and N_A are, respectively, the number-average molar mass, grafting density, bulk density of the grafted polymer, and Avogadro's number). Since the reaction conditions are the same for the entire gradient, the increase of the height of the polymer layer can be correlated with the continuous increase of the grafting density. EBCL thus provides a direct tool to control not only the 2D locus of a grafting point for the SIP process but also, by variation of the locally applied electron dosage, the grafting density, and hence adds a third dimension to the morphology control of structured polymer brushes.

As is apparent from Figures 5 and 6, the height of the gradient polymer brush is not a linear function of the locally applied electron dose but follows, after an induction period between 0 and 5 mC cm^{-2}, an exponential function. (The onset is caused by the fact that the electron-irradiation dwell time had to be optimized for high doses of up to 115 mC cm^{-2} and short writing time. The initial electron dose of <4 mC cm^{-2} cannot be controlled accurately if a maximum final dose of 115 mC cm^{-2} is applied within the same irradiation process.) This dependence agrees with previous ex situ X-ray photoelectron spectroscopy (XPS) and Fourier-transform infrared (FTIR) spectroscopy data on the nitro-to-amino conversion as a function of the applied electron dosage.[9] Moreover, full nitro-to-amino conversion was observed at $\approx$35 mC cm^{-2}, which coincides nicely with the dose corresponding to the maximum height of the polymer-brush layer of $h_d = 380$ nm in the gradient (Figure 5), which we interpret as the gradient area with the maximum grafting density.[9] A similar thickness/dosage dependency was also reported in earlier experiments on the chemical coupling of small molecules to the cABT monolayers created by EBCL at different electron dosages.[28] Also here, the highest grafting densities were observed on the NBT areas irradiated with a dosage between 30 and 50 mC cm^{-2} and primary electron energies of 2.5 keV. The height increase as a function of the electron dosage, $H(D)$, could be fitted exponentially: $H(D) = H_0[1-\exp(-D/D_0)]$, where H_0 is the maximum measured height, D is the applied electron dose, and D_0 is a measure of the process efficiency.

However, the data reported earlier in Reference [9] showed a relatively large scattering because of the ex situ method (e.g., because of surface contamination). To investigate the electron-induced conversion of NBT to cABT, similar but more reliable and detailed XPS characterization of this process was carried out in situ. The irradiation was performed by 10 eV electrons, and the dose was varied from 0 to 120 mC cm^{-2}. Similar to the previous results,[9,27] the N 1s spectra of the irradiated NBT SAMs exhibited the characteristic emission related to the pristine nitro species and irradiation-induced amino species. The intensity of the former and latter emission decreases and increases, respectively, with progressive irradiation following the nitro-to-amino transformation. The respective intensities and the total intensity of the N 1s signal are presented as a function of the irradiation dose in Figure 7a. The extent of the nitro-to-amino conversation derived from the above intensities is plotted in Figure 7b.

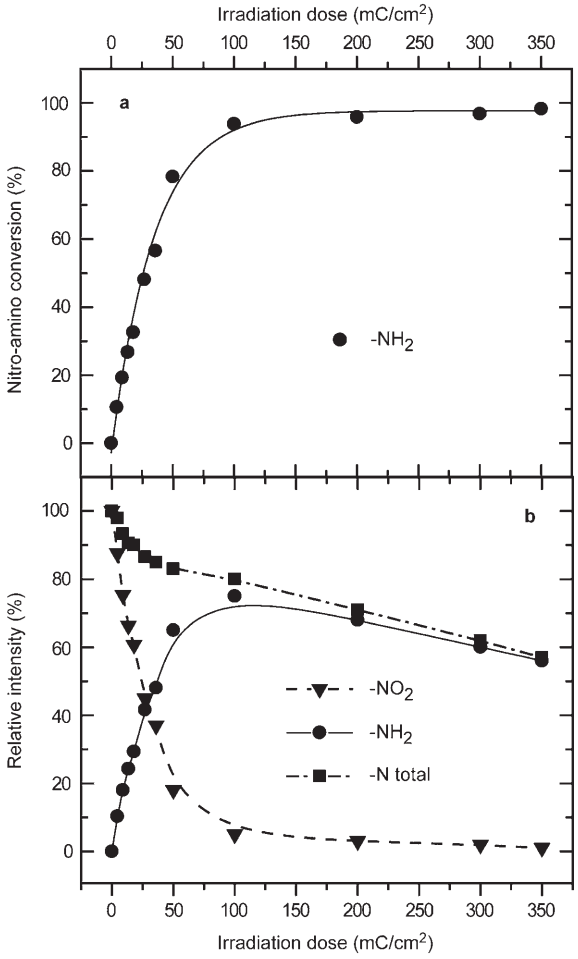

Figure 7. Results of the analysis of the N 1s XPS spectra of the NBT SAMs exposed to 10 eV electrons. a) Extent of the nitro-to-amino conversion derived from the intensities given in (b). b) Intensities of the N 1s emissions related to the nitro and amino groups as well as the total N 1s intensity as functions of irradiation dose

The electron-dosage-dependent conversion of the 4′-nitro group of the NBT monolayer to the 4′-amino group of the resulting cABT SAM follows clearly the exponential function suggested earlier, and corroborates our interpreta-

small NANO MICRO

tion of the direct dependence of the brush height on the locally applied electron dose. Comparison of these in situ results with our previously reported data also reveals more about the dependence of the conversion on the energy of the irradiation used. While the complete NBT-to-cABT conversion is achieved at an electron dosage of $\approx 35\,mC\,cm^{-2}$ and at energies of $\geq 50\,eV$, an irradiation dosage of $\approx 120\,mC\,cm^{-2}$ is needed for the same conversion at electron energy of 10 eV (Figure 7). This result can be explained by the fact that not only the primary but also secondary electrons with energies of 5–10 eV contribute to the conversion. Primary electrons with a higher kinetic energy create a much larger number of secondary electrons (originating mostly from the substrate), and are therefore more efficient for the conversion than electrons of 10 eV energy, which create only a small number of secondary electrons.

As seen in Figure 5, the height of the polymer-brush gradient does not increase monotonously over the entire range of the applied doses. After a maximum polymer layer thickness of 380 nm is reached at a dosage of $\approx 35\,mC\,cm^{-2}$, the thickness slowly but steadily decreases again. Although SAMs with aromatic mesogens show a significantly higher stability towards electron irradiation as compared to alkyl-based monolayers due to the irradiation-induced crosslinking reaction,[29] it was found that terminal functions of biphenyl or terphenyl SAMs are decomposed and desorb from the monolayer at higher dosages and high energies of the primary electrons. This effect was recently reported for thiol-functionalized terphenyl SAMs[30] and was also previously observed for the NBT films.[9] Along with the nitro-to-amino conversion, the total nitrogen content in the latter films was found to decrease slowly with progressive irradiation at high electron dosage. This was attributed to the irradiation-induced desorption of the 4′ function, and was about 11 % of the total nitrogen content at full nitro conversion at an electron energy of 50 eV. Both this behavior and the decrease of the total nitrogen content at the SAM/ambient interface are exactly reproduced by the experimental curves in Figure 7, as far as one scales down the dosage for 10 eV electrons by a correction factor accounting for the dependence of the nitro–amino conversation rate on the primary-electron energy. In Figure 7 a slow but steady decrease of the total nitrogen content is visible, and at a dosage of $120\,mC\,cm^{-2}$ the loss of surface functionality is about 20 % as compared to the value corresponding to the onset of saturation for the nitro-to-amino conversion. For the gradient polymer brush, this means a slower but constant loss of density of the SIP initiators, which results in decreasing polymer grafting density for areas exposed to dosages above 30–$35\,mC\,cm^{-2}$. Indeed, the section analysis in Figure 5 shows a slow and near linear decrease of h_d from 380 nm at $30\,mC\,cm^{-2}$ to 110 nm at $115\,mC\,cm^{-2}$.

Although the grafting-density gradient shows that the height of the polymer brushes is directly related to the surface concentration of amino groups, the possibility that the kinetics of SIPP varies with σ cannot be excluded without measuring the molar masses of the grafted brushes. This issue has been pointed out by Genzer et al.[15] for the polymerization of acrylamide by atom-transfer radical polymerization (ATRP) on initiator gradient substrates. However, their data indicated that the degree of polymerization of the grafted polymers was not noticeably affected by the local initiator concentration. In contrast to this finding, a recent study[31] reports a complex, nonlinear relationship between the film growth rate and the initiator density. Also in this case, ATRP (of 2-hydroxyethyl methacrylate) was used as the SIP reaction. While the film growth rate is constant with the polymerization time, which suggests good control of the radical polymerization, the dependence on the surface initiator concentration suggested a significant influence of the bimolecular termination reaction due to the high local radical concentration at the surface. As in the SIPP reaction presented here, the polymerization proceeds via a free-radical mechanism and, moreover, free polymerization occurs in the monomer solution. Hence a grafting of growing polymer chains onto the surface may occur, and therefore the above-mentioned results are not directly applicable. Considering this, the good control of the layer morphology by a free-radical polymerization technique becomes even more surprising.

At this point, it can be concluded that it is possible to fine tune the morphology of a polymer brush with EBCL by controlling the local grafting density for the free-radical SIPP. Alternatively, the brush height is, within a broad reaction-time window, a linear function of the UV irradiation/polymerization time. These two parameters already allow a fine-tuning of the general morphology of polymer layers and even the control of individual structures on a substrate, as demonstrated by the brush gradient.

Recently, Patra and Linse[32,33] performed computer-simulation studies to correlate the width of a nanostructured polymer brush with a given degree of polymerization to the resulting height of the structure. Since for nanostructured brushes, the length of the grafted macromolecules is comparable to the dimension of the lateral structures, the height is a function of the width because of the instant drop of the local grafting density at the edges. This allows a conformational relaxation of the stretched chains within the brush and, therefore, a decrease of the brush height. These theoretical studies were corroborated by recent experimental findings in co-operation with the group of Zauscher.[21]

For a quantitative study of the effect of the e-beam dose and the initial structure widths on the resulting brush morphology, we created an array of isolated structures by varying the irradiation dosage as well as the feature diameter over the entire pattern. This excludes known proximity effects of the electron irradiation in densely patterned regions. Furthermore, the local brush height of a continuous-gradient pattern is always influenced by the brush grafting density in the vicinity, and the study of isolated patterns gives a more precise relationship between the patterning parameters and the resulting brush morphology.

Figure 8 shows the AFM image of the fabricated polymer-brush array with systematic variation of the electron dosage from 5 to $100\,mC\,cm^{-2}$ and a dot diameter from 50 to 1000 nm. In Figure 9, the maximum heights of the polystyrene dots are plotted as functions of the electron irradiation dosage for structures of the respective primary diame-

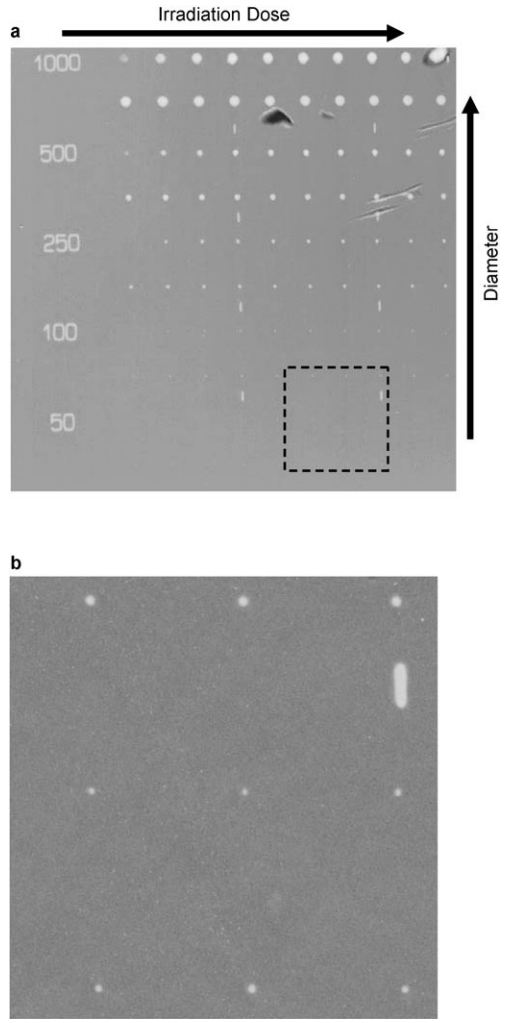

Figure 8. AFM image ($50 \times 50\ \mu m^2$) of an array of structured polystyrene brushes recorded in tapping mode under ambient conditions. a) Dots with a diameter of 1000, 500, 250, 100, and 50 nm and an electron irradiation dose of 5 to 100 $mC\,cm^{-2}$ were patterned on an NBT SAM on gold. The patterns were then amplified by the SIPP of styrene. b) Detailed second AFM scan of the $12 \times 12\ \mu m^2$ area indicated in (a), which shows three 100-nm dots at a radiation dose of 85, 87.5, and 90 $mC\,cm^{-2}$ (top row, from left to right) and six dots with a diameter of 50 nm (middle row: irradiation dose 35, 37.5, and 40 $mC\,cm^{-2}$; bottom row: irradiation dose 85, 87.5, and 90 $mC\,cm^{-2}$). The visible stripe was created intentionally for orientation within the array.

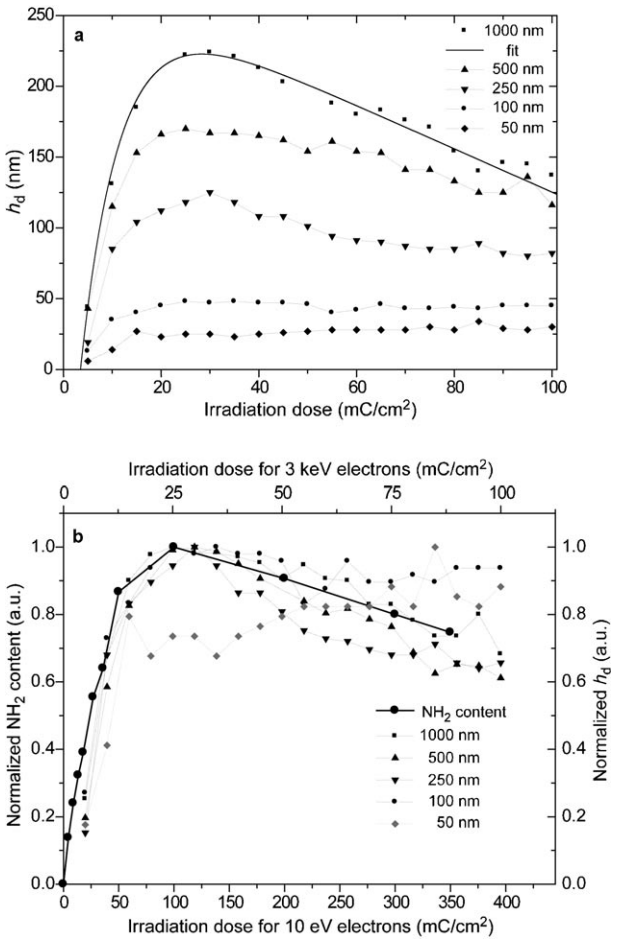

Figure 9. a) Height of the polymer-brush dots shown in Figure 8 as a function of electron irradiation dose for dots with diameters of 50, 100, 250, 500, and 1000 nm (polymerization time = 16 h). The fit function used for the data series with $d = 1000$ nm is $h_d(D) = h_{d0}[1-\exp(-D'/D_0)] - D'S$ (see text for details). The values used were $h_{d0} = 273$ nm, $D' = D - 3.5\ mC\,cm^{-2}$, $D_0 = 8\ mC\,cm^{-2}$, and $S = 1.53\ nm\,mC\,cm^{-2}$. b) Unified plot of the normalized h_d and normalized amino-group content versus the irradiation dose for all structures.

ters. Qualitatively, the same dosage/height dependence as in the grafting gradient experiment can be observed. Between a dosage of 0 and 30 $mC\,cm^{-2}$, h_d increases strongly with the dosage and the thickest polymer brushes were obtained at a dosage of 30 $mC\,cm^{-2}$. Also, a steady decrease of h_d at dosages above 30 $mC\,cm^{-2}$ is visible, which reflects the constant reduction of the grafting site density due to the desorption of the 4′ functionality of the SAM. Moreover, the dependence of height on the applied dosage value and, thus, the local grafting density is more pronounced for larger structures.

The measured polymer-brush thickness as a function of the irradiation dosage in the EBCL step can be fitted by using the function $h_d(D) = h_{d0}[1-\exp(-D'/D_0)] - D'S$, where h_d is the dry brush height, h_{d0} is the brush height at maximum NBT-to-cABT conversion, D' is the onset corrected dosage, D_0 describes the efficiency of the conversion, and S is the stability factor describing the radiation-induced damage of the monolayer template. The exponential term of the fit function ($h_{d0}[1-\exp(-D'/D_0)]$) describes the electron-irradiation-induced conversion of the 4′-nitro to the 4′-amino group according to Gölzhäuser et al.[28] The second linear term ($-D'S$) relates to the steady decomposition of any chemical functionality upon electron irradiation (see fit for the data series for $d = 1000$ nm in Figure 9a). This equation describes the effective initiator (precursor) density for the SIPP process created by the EBCL. The good agreement of the fit with the experimental data unambiguously shows that EBCL controls the local initiator density and, in consequence, the grafting density and height of the resulting brush. The direct correlation between the polymer-brush

NANO MICRO small

height and the surface amino-group concentration, as created by EBCL, is summarized in Figure 9b. The correlation is good for structures with $d = 1000$–250 nm. As the individual dots become smaller, the influence of the structure footprint size on the layer thickness becomes apparent. As a result of the normalization, the scattering of the height values increases for layer thicknesses below 30 nm.

The strong dependence of the resulting h_d on the lateral structure size of the polymer-brush dots (see Figure 8) is illustrated in Figure 10. These results are in agreement with

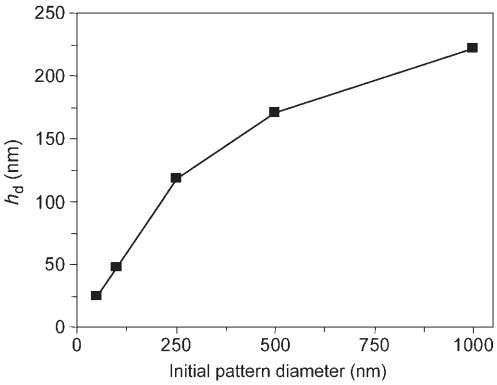

Figure 10. Maximum thickness of the polystyrene brush as a function of the initial pattern size (dot diameter). The layer thickness of polystyrene brushes formed under identical conditions (dose = 25 mC cm^{-2}; polymerization time = 16 h) in the gradient (Figure 5) was 370–375 nm.

the recent results by Zauscher et al.[21] This behavior can be explained by considering that grafted polymers located at the border of the structures extend to the polymer-free surface to minimize entropic energy. This leads to less chain crowding and, thus, less chain stretching in the vicinity and consequently to a lower h_d. Such a relaxation becomes more effective as the structures become smaller. Interestingly, for 0.5- and 1-μm structures, h_d still increases significantly. This long-range phenomenon probably underlines the highly cooperative effect within dense polymer brushes, and Zauscher et al.[21] reported an influence of the pattern diameter on the brush height for diameters up to 3 μm. The effect of the variation of the lateral structure size on h_d is also significant when we compare the brush height in the arrays (Figure 8) and in the gradient (Figure 5). While an electron dosage of 25 mC cm^{-2} creates layer thicknesses from 25 to 222 nm for the dot array, h_d in the grafting density gradient (10×50 μm^2) was measured as 370–375 nm for the area irradiated with the same electron dosage and same energies. Note that the gradient and the array depicted in Figures 5 to 8 are from the identical substrate and, thus, identical reaction conditions were applied.

The possibility of the brushes extending to polymer-free surface regions also results in a widening of the structures. In recent studies by Zauscher and co-workers on the impact of the structure footprint on the resulting polymer-brush morphology this issue could not be addressed, because there the brushes are located on "…gold features raised above the background by ≈40 nm, which results in additional lateral growth of polymer brushes."[21c]

In Table 1, the width at half maximum height ($w_{1/2}$) of the dot structures created under identical polymerization conditions and dosage (25 mC cm^{-2}) were measured by AFM and are compared to the diameter of the patterns created by EBCL. The values in Table 1 show that the lateral broadening of the structures is about 100 nm and nearly independent of the pattern diameter. This result indicates that the individual polymer chain growth is not affected by the respective structure size.

Table 1. Lateral dimensions of nanopatterned polystyrene brushes compared to the original feature diameter created by EBCL (d = diameter of the pattern created by EBCL, $w_{1/2}$ = width at half maximum height of the polymeric structures).

d [nm]	$w_{1/2}$ [nm]	$w_{1/2} - d$ [nm]
1000	1099	99
500	600	100
250	337	87
100	209	109
50	156	106

3. Conclusions

Ex situ kinetic studies of the SIPP process on structured SAMs of cAMBT revealed a linear increase of the polymer-brush thickness with the UV irradiation/polymerization time over a wide reaction-time window. Furthermore, the effect of the applied electron dosage on the thickness of the brush layer was studied. The correlation between the dosage-dependent conversion of the 4′-nitro to the 4′-amino group and the layer thickness of the resulting polymer brush leads to the conclusion that the polymer-brush grafting density, and thus the brush height, can be directly controlled by the EBCL process. This allowed the fabrication of defined grafting-density gradients on the micrometer scale.

Besides gradient structures, structure arrays were prepared for the combinatorial study of the effect of the lateral structure size and the irradiation dosage on the morphology of the resulting polymer-brush layer. Analysis of these arrays revealed the dependence of h_d on both electron dosage and the structure width.

This unique combination of EBCL as a lithographic technique to locally manipulate the surface chemistry and SIP to amplify the created differences allows the preparation of polymer-brush layers of controlled morphologies in three dimensions. We are currently investigating the possibility of creating more complex 3D architectures on the micro- and nanometer scales using the correlations found.

4. Experimental Section

SAM preparation: The preparation of the NBT SAMs,[11] methyl malonodinitrile, and the surface-bonded initiator (cAMBT)[34] were performed as previously reported.

EBCL: A flood gun (50 eV, 60 mC cm^{-2}) was used to irradiate the NBT SAMs through a stencil mask (Quantifoil Micro Tools, Jena; hole radius: 1 μm, center-to-center distance: 4 μm) placed directly onto the substrate. The dose for EBCL writing was calibrated by using a Faraday cup placed on the same holder as the SAM samples. The accuracy of the calibration was better than 5–10%. Direct writing with a focused e-beam was performed with a LEO 1530 SEM with Raith Elphy Plus pattern generator system (REPGS) software. The e-beam energy was set at 3 keV; the base pressure during the irradiation was $\approx 5 \times 10^{-6}$ mbar. For fabrication of the polymer-brush gradient, 100 parallel lines each of width 500 nm were written with a focused beam using a step size typically between 5 and 20 nm and a beam current between 10 and 400 pA.

In situ XPS studies: For XPS monitoring of the chemical changes upon irradiation, pristine NBT SAMs were irradiated with 10 eV electrons. The doses were estimated by multiplication of the exposure time by the current density ($\approx$19 μA cm^{-2}). The electron gun was mounted at a distance of $\approx$15 cm from the sample to ensure uniform illumination. The base pressure in the chamber during irradiation was 1×10^{-8} mbar. The irradiation dose was calibrated using a Faraday cup. The accuracy of the calibration was better than 5–10%.

The XPS characterization was performed immediately after irradiation, without exposure of the irradiated films to ambient conditions. The measurements were performed with an Al Kα X-ray source and an LHS 11 analyzer. The acquisition of spectra was carried out in normal emission geometry with an energy resolution of $\approx$1.0 eV. The X-ray source was operated at a power of 260 W and positioned $\approx$1.5 cm away from the samples. The energy scale was referenced to the Au $4f_{7/2}$ peak of alkanethiolate-coated gold at a binding energy of 84.0 eV.[35] For each sample, a wide-scan spectrum and the C 1s, N 1s, and Au 4f narrow-scan spectra were measured. Emphasis was placed on the N 1s spectra, since they provided direct information on the chemical identity of the SAM/ambient interface, which is of major importance for SIP.

The XPS spectra were fitted by symmetric Voigt functions using a Shirley-type background. The fits were performed self-consistently; the same fit parameters were used for identical spectral regions.[35]

SIPP: A freshly prepared SAM of cAMBT was submerged in approximately 2 mL of freshly distilled and degassed styrene (Fluka) in a glass photoreaction vial. Polymerization was allowed to complete within different time periods (0–25 h) under irradiation with UV light ($\lambda_{max} = 350$ nm, 9.2 mW cm^{-2}) in a Rayonet photochemical reaction chamber (Branford, Connecticut) at room temperature. After photopolymerization, the samples were removed from the reaction solution and immediately washed with toluene. To ensure that only chemically grafted polystyrene remained on the surface, all substrates were additionally cleaned by Soxhlet extraction with toluene overnight.

AFM: AFM images were acquired in tapping mode with a Nanoscope IIIa scanning probe microscope (Veeco Instruments); standard cantilevers were used. The thickness of the polymer layer was evaluated from 20 × 20-μm^2 scans of structured polymer surfaces (radius 1 μm). In most cases, image analysis was performed on raw data sets; however, in some selected cases the images had to be smoothed by the software routine provided with the instrument. The topography of the structured surfaces was analyzed using the depth analysis routine of the software. Here, two distinct populations of the height distribution were found (one for the bare substrate including substrate surface roughness and one for the polymer structure plateaus including edge bias and roughness, see Figure 2). The difference between the maxima of both distributions was taken as the average height of the polymer-brush features. The given error σ (Figures 2 and 3) was taken from the distribution originating from the polymer features. Thus, the structure quality (bias, height distribution of single and all structures) and surface roughness of the polymer features were taken into account.

Acknowledgements

The authors acknowledge the financial support of the Deutsche Forschungsgemeinschaft (JO287/2-1, GR625/50-1, and ZH 63/9-2), the SFB 563 "Bioorganic Functional Systems on Solids" (TP: Jordan A8), and the EU Integrated Project "Ambio" (M.G. and A.K.). We thank the Physikalisch Technische Bundesanstalt for providing the patterned Au/Pd substrates. R.J. and M.G. are grateful to the "Fonds der Chemischen Industrie" for financial support.

[1] *Surface-Initiated Polymerization I & II* (Ed.: R. Jordan) **2006**, Springer, Berlin.
[2] a) R. Laible, K. Hamann, *Adv. Colloid Interface Sci.* **1980**, *13*, 65; b) O. Prucker, J. Rühe, *Macromolecules* **1998**, *31*, 592.
[3] a) B. Zhao, W. J. Brittain, *J. Am. Chem. Soc.* **1999**, *121*, 3557; b) K. Matyjaszewski, P. J. Miller, N. Shukla, B. Immaraporn, A. Gelman, B. B. Luokala, T. M. Siclvan, G. Kickelbick, T. Vallant, H. Hoffmann, T. Pakula, *Macromolecules* **1999**, *32*, 8716.
[4] R. Jordan, A. Ulman, J. F. Kang, M. Rafailovich, J. Sokolov, *J. Am. Chem. Soc.* **1999**, *121*, 1016.
[5] a) R. Jordan, A. Ulman, *J. Am. Chem. Soc.* **1998**, *120*, 243; b) R. Jordan, N. West, A. Ulman, Y. M. Chou, O. Nuyken, *Macromolecules* **2001**, *34*, 1606.
[6] G. M. Whitesides, Y. Xia, *Angew. Chem.* **1998**, *110*, 568; *Angew. Chem. Int. Ed.* **1998**, *37*, 550.
[7] B. Liederberg, P. Tengvall, *Langmuir* **1995**, *11*, 3821.
[8] C. A. Mirkin, S. Hong, L. Demers, *ChemPhysChem* **2001**, *2*, 37.
[9] W. Eck, V. Stadler, W. Geyer, M. Zharnikov, A. Gölzhäuser, M. Grunze, *Adv. Mater.* **2000**, *12*, 805.
[10] W. Geyer, V. Stadler, W. Eck, M. Zharnikov, A. Gölzhäuser, M. Grunze, *Appl. Phys. Lett.* **1999**, *75*, 2401.
[11] U. Schmelmer, R. Jordan, W. Geyer, W. Eck, A. Gölzhäuser, M. Grunze, A. Ulman, *Angew. Chem.* **2003**, *115*, 577; *Angew. Chem. Int. Ed.* **2003**, *42*, 559.
[12] a) J. F. Kang, A. Ulman, S. Liao, R. Jordan, G. Yang, G. Y. Liu, *Langmuir* **2001**, *17*, 95; b) J. F. Kang, A. Ulman, S. Liao, R. Jordan, *Langmuir* **1999**, *15*, 2095.
[13] W. Eck, A. Küller, M. Grunze, B. Völkel, A. Gölzhäuser, *Adv. Mater.* **2005**, *17*, 2583.
[14] U. Schmelmer, A. Paul, A. Küller, M. Steenackers, A. Ulman, M. Grunze, A. Gölzhäuser, R. Jordan, *Small* **2007**, *3*, 459.
[15] R. R. Baht, M. R. Tomlinson, T. Wu, J. Genzer, *Adv. Polym. Sci.* **2006**, *198*, 51, and references therein.
[16] a) C. Xu, T. Wu, C. M. Drain, J. D. Batteas, M. J. Fasolka, K. L. Beers *Macromolecules* **2006**, *39*, 3359; b) C. Xu, T. Wu, J. D.

Batteas, C. M. Drain, K. L. Beers, M. J. Fasolka *Appl. Surf. Sci.* **2006**, *252*, 2529; c) C. Xu, S. E. Barnes, T. Wu, D. A. Fischer, D. M. DeLongchamp, J. D. Batteas, K. L. Beers *Adv. Mater.* **2006**, *18*, 1427.
[17] B. P. Harris, A. T. Metters *Macromolecules* **2006**, *39*, 2764.
[18] B. Zhao, *Langmuir* **2004**, *20*, 11748.
[19] T. Matsuda, *Adv. Polym. Sci.* **2006**, *197*, 67, and references therein.
[20] a) M. Kaholek, W.-K. Lee, S.-J. Ahn, H. Ma, K. C. Caster, B. LaMattina, S. Zauscher, *Chem. Mater.* **2004**, *16*, 3688; b) S.-J. Ahn, M. Kaholek, W.-K. Lee, B. LaMattina, T. H. LaBean, S. Zauscher, *Adv. Mater.* **2004**, *16*, 2141; c) M. Kaholek, W.-K. Lee, B. LaMattina, K. C. Caster, S. Zauscher, *Nano Lett.* **2004**, *4*, 373.
[21] a) M. Kaholek, W.-K. Lee, J. Feng, B. LaMattina, D. J. Dyer, S. Zauscher, *Chem. Mater.* **2006**, *18*, 3660; b) W.-K. Lee, M. Kaholek, S.-J. Ahn, M. Patra, P. Linse, S. Zauscher, *Polymer Prepr.* **2005**, *46*, 74; c) W.-K. Lee, M. Patra, P. Linse, S. Zauscher, *Small* **2007**, *3*, 63.
[22] R. Kerber, O. Nuyken, R. Steinhausen, *Makromol. Chem.* **1976**, *177*, 1357.
[23] O. Prucker, J. Habicht, I. J. Park, J. Rühe, *Mater. Sci. Eng. C* **1999**, *8–9*, 291.
[24] U. Schmelmer, A. Paul, A. Küller, R. Jordan, A. Gölzhäuser, M. Grunze, A. Ulman, *Macromol. Symp.* **2004**, *217*, 223.
[25] D. J. Dyer, J. Feng, R. Schmidt, V. N. Wong, T. Thao, Y. Yagci, *Macromolecules* **2004**, *37*, 7072.
[26] D. J. Dyer, J. Feng, C. Fivelson, R. Paul, R. Schmidt, T. Zhao in *Polymer Brushes* (Eds.: R. C. Advincula, W. J. Brittain, K. C. Caster, J. Rühe), Wiley-VCH, Weinheim, Germany **2004**, p. 129.
[27] M. Zharnikov, A. Shaporenko, A. Paul, A. Gölzhäuser, A. Scholl, *J. Phys. Chem. B* **2005**, *109*, 5168.
[28] W. Geyer, V. Stadler, W. Eck, A. Gölzhäuser, M. Grunze *J. Vac. Sci. Technol. B* **2001**, *19*, 2732.
[29] M. Zharnikov, M. Grunze, *J. Vac. Sci. Technol. A* **2002**, *20*, 1793.
[30] Y. Tai, A. Shaporenko, M. Grunze, M. Zharnikov, *J. Phys. Chem. B* **2005**, *109*, 19411.
[31] Z. Bao, M. L. Bruening, G. L. Baker, *Macromolecules* **2006**, *39*, 5251.
[32] M. Patra, P. Linse, *Nano Lett.* **2006**, *6*, 133.
[33] M. Patra, P. Linse, *Macromolecules* **2006**, *39*, 4540.
[34] A. Gölzhäuser, W. Eck, W. Geyer, V. Stadler, T. Weimann, P. Hinze, M. Grunze, *Adv. Mater.* **2001**, *13*, 806.
[35] J. F. Moulder, W. E. Stickle, P. E. Sobol, K. D. Bomben, *Handbook of X-ray Photoelectron Spectroscopy* (Ed.: J. Chastian), Perkin–Elmer Corp., Eden Prairie, MN, **1992**.

Received: March 14, 2007
Revised: July 23, 2007
Published online on September 13, 2007

